Structural Optimization Design and Analysis of the Spraying-Plastering Integrated Robot Nozzle

Liming Si, Zhibin Yao *

School of Mechanical Engineering, Taiyuan University of Science and Technology, Taiyuan, China, 030024

* Corresponding Author Email: yzb@tyust.edu.cn

Abstract. As a core surface treatment process in modern industry, electrostatic powder spraying technology demands high coating quality; however, integrated spraying-plastering robots frequently encounter powder accumulation issues in electrostatic devices and nozzles, adversely affecting spraying efficiency, coating uniformity, and equipment lifespan. This study establishes a three-dimensional nozzle model using SolidWorks, and employs ANSYS FLUENT for multiphysics coupling simulations to analyze structural deficiencies in the original design and propose rational optimization schemes. By reconstructing the single-beam electrostatic device into three slender beams arranged in an equilateral triangular distribution (1 mm in width) and adopting a conical inner cylinder design, the gas flow characteristics and powder distribution uniformity are significantly improved. Static analysis shows that the maximum stress of the optimized nozzle is reduced from 0.2627 MPa to 0.1436 MPa, with deformation decreased by 59.8%, which is far below the material's safety threshold. Fluid dynamics simulations verify the airflow stability of the optimized structure; both single-phase flow and discrete phase models demonstrate a 31% improvement in the uniformity of outlet velocity distribution, with reduced powder retention. This study offers valuable insights for the high-efficiency and low-energy-consumption design and structural optimization of integrated spraying-plastering robot nozzles.

Keywords: Spraying Robot, Structural Optimization, Fluid Simulation, Electrostatic Device, Powder Accumulation.

1. Introduction

Since its industrial application in the 1980s, electrostatic powder spraying technology has rapidly become a core surface treatment process in fields such as automobile manufacturing, home appliance production, and electronic packaging, due to its high efficiency, environmental friendliness, and excellent coating performance [1]. The technology utilizes a high-voltage electrostatic field ranging from tens of thousands to hundreds of thousands of volts to ensure the uniform adsorption of charged powder coatings onto the workpiece surface under Coulomb force, followed by heating and baking to cure the powder molecules, forming a firm bond on the surface [2]. Compared with traditional solvent-based coatings, it reduces volatile organic compound (VOC) emissions by more than 90% and is virtually VOC-free [3]. According to industry estimates (QY Research, 2025), electrostatic powder spraying technology can reduce global VOC emissions by approximately 600,000 tons annually, equivalent to 1.5 million tons of carbon dioxide emissions [4]. Electrostatic spraying, as an environmentally prioritized surface treatment, has garnered increasing attention for it’s near-zero VOC emissions and >95% material utilization enabled by electrostatic adsorption, high-temperature curing, and closed-loop powder recycling. Nevertheless, inherent nozzle design flaws causing persistent powder accumulation demand targeted structural modifications to holistically advance sustainability, coating performance, and economic viability [5-8].

Traditional nozzle designs have long relied on empirical formulas and trial-and-error methods, lacking detailed analysis of the internal flow field, which results in low spraying efficiency and limited equipment lifespan. For example, Zhang et al. found through experimental studies that early electrostatic powder spraying equipment suffered from unreasonable nozzle geometry design, causing powder particles to frequently collide with the wall during ejection and accumulate in large quantities on the inner side of the electrostatic device's crossbeam. Since the flat nozzle only has an opening in the middle, the other unopened areas obstruct fluid flow, causing a decrease in flow velocity at these regions and leading to powder accumulation [9]. Furthermore, traditional single-crossbeam electrostatic devices (with a crossbeam width of 4 mm) are prone to vortex formation under high-speed airflow (10 m/s); the core pressure of these vortices is lower than that of the mainstream region, causing powder particles to be retained and gradually form a dense accumulation layer, eventually blocking the flow channel. Concurrent parametric optimization studies further inform structural enhancements: Chen demonstrated optimal first-pass efficiency with 30-50μm particles in conventional spraying, while combining ≤30μm fines with limited ultrafine particles (≤10μm) improves hard-to-reach area coverage [10]. Liu et al. developed a synergistic spraying voltage-flow field optimization strategy for proton exchange membrane fuel cells, effectively suppressing platinum-carbon agglomeration and improving pore uniformity, thereby advancing a cross-disciplinary framework for innovative spraying technologies [11]. These findings indicate that structural optimization requires dynamic coordination with process parameters (particle size distribution, electrostatic field intensity) to achieve comprehensive spraying efficiency improvements. Boer Jozsef's holistic parameter monitoring system [12] complements our multiphysics-based structural optimization strategy - the former enhances systemic efficiency through closed-loop process control, while the latter resolves structural limitations via flow field reconstruction and mechanical reinforcement, collectively advancing green manufacturing and cost-performance optimization.

In response to the issues, this study explores a multidimensional approach to nozzle structure optimization. The innovation lies in combining an equilateral triangular crossbeam array with a conical inner cylinder design for the first time, alongside adjustments to the nozzle slope angle and flow channel geometry. A comprehensive evaluation of the nozzle structure was conducted based on static analysis, integrated with fatigue life prediction techniques to ensure long-term stability of the optimized design. This design approach effectively reduces turbulence energy in the flow field, minimizes powder accumulation inside the nozzle, and thereby enhances the stability and consistency of the spraying process. It achieves a synergistic optimization of flow field uniformity and structural strength, and its engineering feasibility has been verified through multiphysics simulation technology. This innovative achievement offers novel approaches and methodologies for optimizing nozzle structure design, demonstrating promising application prospects and practical significance.

2. Materials and Methods

2.1. Model Formulation

To facilitate comprehensive analysis of powder accumulation behavior and subsequent investigations, computational modeling of the spray device was implemented, with this paper focusing on presenting the three-dimensional model of the nozzle section where critical phenomena predominantly occur. The primary components of the nozzle structure include the spray nozzle and the electrostatic device. A three-dimensional model of the nozzle was established using SolidWorks, as shown in Fig 1. Which includes the electrostatic device, nozzle and internal flow channel. In the original design, the electrostatic device employed a single 4 mm-wide crossbeam, the nozzle featured a flat structure, and the internal flow channel adopted a trapezoidal cross-section.

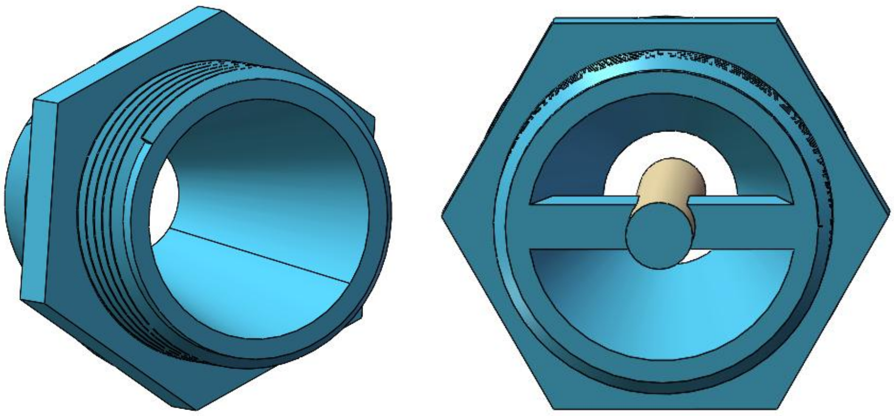

Fig 1. Three-Dimensional Model of the Original Nozzle.

Some of the main dimensional parameters of the model are listed in Table 1.

Table 1. Dimensional Parameters of the Original Model.

Dimension Name	Dimensional Parameters
Nozzle Diameter	12mm
Inlet Diameter	24mm
Pipe Inclination Angle	60°
Nozzle Length	33mm
Length of Electrostatic Device Core	50mm
Core Diameter	6mm
Crossbeam Width	4mm

To validate the structural rationality, a static analysis of the model was conducted using ANSYS. The calculated strain and stress results are shown in Fig 2., with a maximum stress of 0.2627 MPa and a maximum deformation of 2.4367E-6 m. Considering that the tensile yield strength of typical plastics is 40 MPa [13] and the maximum allowable deformation is less than or equal to 5% [14] (2E-6 m), the stress is far below the specified threshold. However, deformation exceeds acceptable limits, necessitating further optimization to reduce structural deformation and enhance mechanical performance.

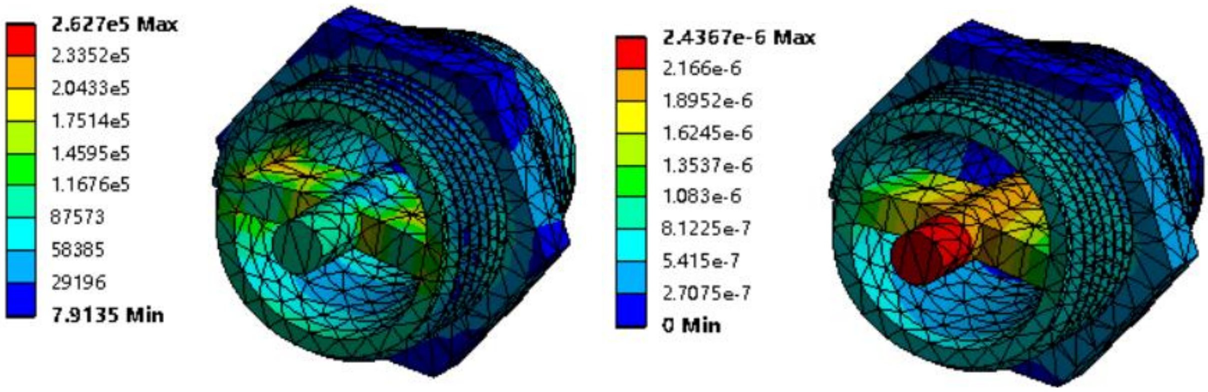

(a) Stress Distribution. (b) Deformation Distribution.

Fig 2. Stress Distribution and Deformation Distribution of the Original Model.

First, the powder spraying process is analyzed: the powder flows out from the interior of the electrostatic device, enters the nozzle, and is then ejected through the nozzle outlet. As the upper part of the nozzle is precisely connected to the electrostatic device, the analysis focuses on the internal structure of the electrostatic device, the nozzle geometry, and the internal conditions near the nozzle. Flow field simulations based on two models in ANSYS FLUENT demonstrate that unreasonable settings of the plastic crossbeam width parameter in the electrostatic device's internal structure lead to flow field turbulence (Figs. 3(a), and 4(a).) and uneven pressure distribution within the nozzle (Figs. 3(b), and 4(b).) As shown in Fig 3(a)., when the crossbeam dimension exceeds the critical value, the flow field exhibits an obvious velocity gradient distribution: the fluid velocity in the core region of the electrostatic device drops to 8–12 m/s, while the adjacent intermediate channel region reaches 45–56 m/s, forming a localized high-speed flow zone. This velocity distribution heterogeneity is further reflected in the asymmetrical pressure field across the nozzle section, as shown in Fig 3(b). Where the pressure difference can reach 1200–1500 Pa.

A comparative analysis of the geometric features of the original 3D structural model (Fig 1.) reveals that the thickened crossbeam design (crossbeam width of 4 mm), adopted to enhance structural stability, introduces fluid dynamic flaws. The distance between the crossbeam and the feed inlet is only 30 mm, and a 60° sharp-angle structure is formed at the connection between the crossbeam and the core of the internal structure (a geometric discontinuity zone). Numerical simulation results indicate that these structural features cause several adverse effects when the two-phase flow (air-powder) passes through: a sudden reduction in flow cross-sectional area triggers boundary layer separation; the sharp-angle region forms a localized backflow zone, increasing the probability of powder particle retention; and a flow velocity attenuation peak appears 3 mm downstream of the feed inlet. These fluid dynamic characteristics are significantly correlated with the phenomenon of powder accumulation.

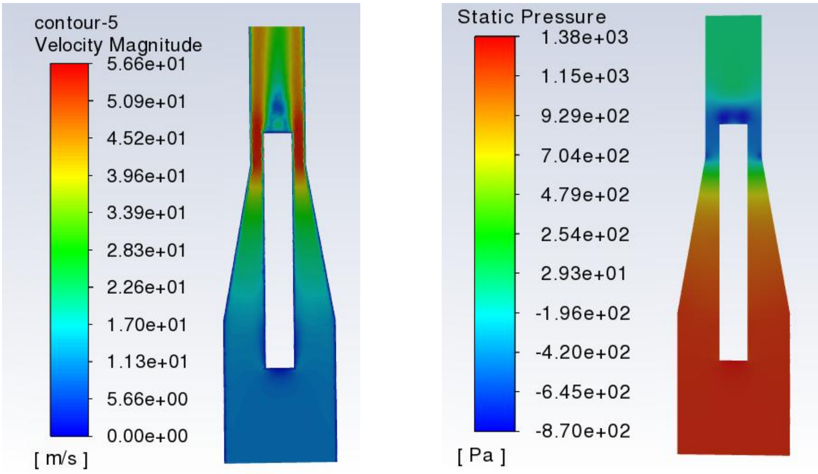

(a) Velocity Contour (b) Pressure Contour

Fig 3. Velocity and Pressure Contours of the Discrete Phase in the Original Model.

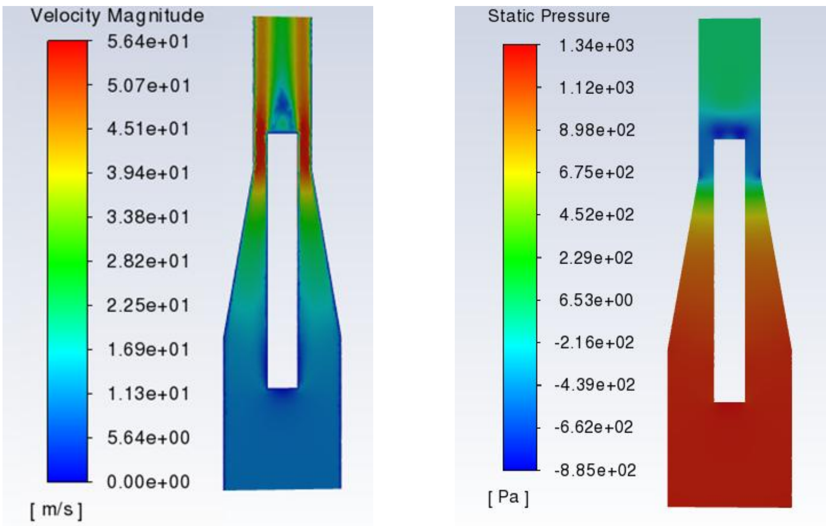

(a) Velocity Contour (b) Pressure Contour

Fig 4. Velocity and Pressure Contours of Single-Phase Flow in the Original Model.

2.2. Optimization Design of the Electrostatic Device

The previous analysis indicated that the excessive width of the electrostatic device's crossbeam impedes fluid flow, increases powder accumulation on the inner side of the crossbeam during spraying, and leads to excessive deformation and unstable structural performance according to static analysis results. To enhance the stability of the internal flow field in the electrostatic device and reduce powder accumulation, targeted optimization of the internal core structure is required. First, the geometric dimensions of the leading surface of the internal core are reduced to minimize flow disturbance, and the sharp angle transitions at the connection between the support structure and the internal core are eliminated. As shown in Fig 5. The original 4 mm wide single crossbeam was restructured into an equilateral triangular support array composed of three 1 mm slender beams. This topological structure significantly reduces the cross-sectional area facing the flow while maintaining mechanical strength and decreases flow channel resistance through symmetrical arrangement.

Furthermore, a conical design is adopted instead of the traditional cylindrical internal core, using a 20° taper to guide the powder towards the central region. Numerical simulations demonstrate that the conical structure generates a stable axial pressure gradient, effectively enhancing the synergistic movement of the powder-air two-phase flow. The optimized composite structure not only strengthens the mechanical stability of the support system but also significantly suppresses flow field turbulence and improves powder transport efficiency.

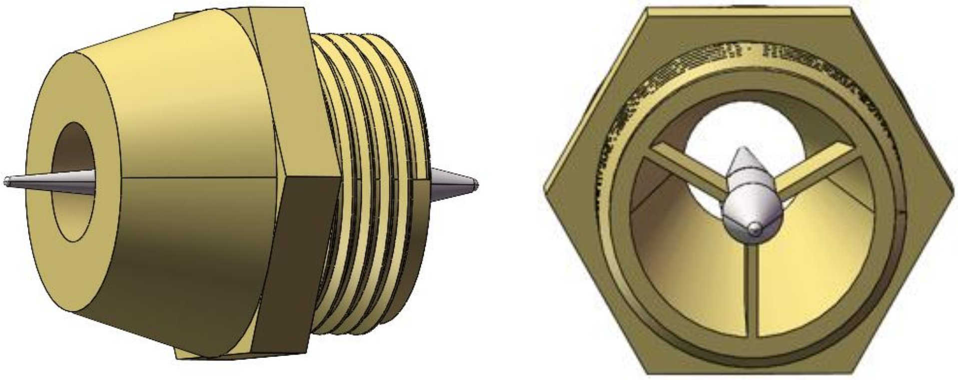

Fig 5. Three-Dimensional Model after Optimization.

The basic dimensional parameters of the optimized model are shown in Table 2.

Table 2. Dimensional Parameters of the Optimized Model.

Dimension Name	Dimensional Parameters
Nozzle Diameter	12mm
Inlet Diameter	24mm
Pipe Inclination Angle	60°
Nozzle Length	33mm
Length of Electrostatic Device Core	50mm
Core Diameter	6mm
Cone Angle	20°
Crossbeam Width	1mm

2.3. Verification and Analysis of the Optimization Scheme

To verify whether the optimized electrostatic device meets the requirements, a static analysis was performed on the optimized device. (Fig 6.) The results show that the maximum stress is 0.14359 MPa and the maximum deformation is 9.8036E-7 m. Compared to the results in Fig 2. Both stress and strain are reduced in the optimized model, improving structural performance and extending its service life. The stress remains well below the plastic yield strength (40 MPa), and the maximum deformation rate is less than or equal to 5% (2E-6 m), indicating that the design meets the requirements.

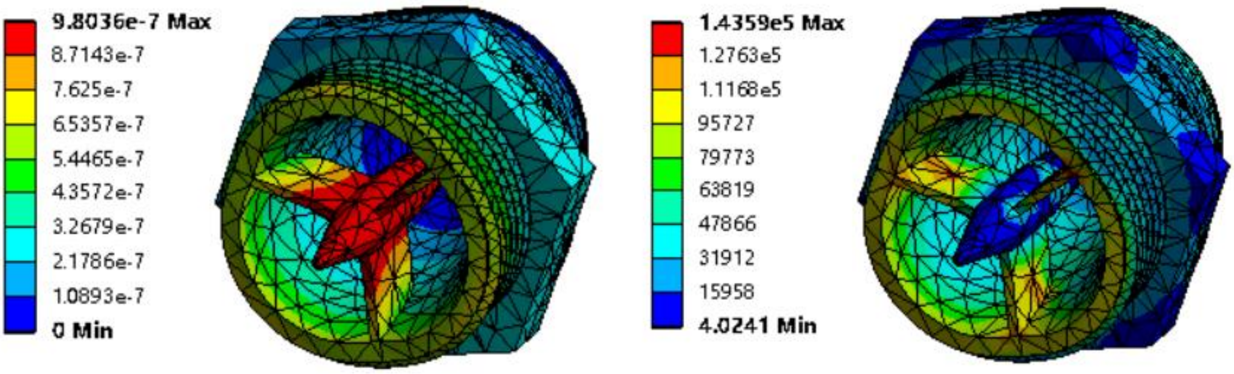

(a) Deformation Distribution. (b) Stress Distribution.

Fig 6. Deformation and Stress Distribution of the Optimized Model.

To further verify the feasibility of the optimization scheme, fluid dynamics simulations were conducted on the optimized nozzle. The single-phase flow model serves as the basis for gas-solid two-phase flow; it is necessary to first ensure the rationality of the airflow field through single-phase flow analysis, such as confirming the absence of backflow and uniform fluid velocity distribution, before performing DPM (Discrete Phase Model) analysis by introducing particles. If the particles have a negligible effect on the airflow (e.g., low-concentration powder), the single-phase flow results can be used as a fixed background flow field to drive particle motion (one-way coupling). If the particle concentration is high or the particle momentum significantly affects airflow (e.g., large-particle spraying), real-time updates (two-way coupling) are required, significantly increasing computational complexity. Both approaches ultimately serve the optimization of the powder spraying process: single-phase flow ensures airflow stability, while two-phase flow ensures efficient powder deposition, jointly reducing defects (such as orange peel and sagging) and minimizing material waste. If the airflow field itself is flawed, the simulation results of particle trajectories will be unreliable. Accordingly, the single-phase flow model is first employed for analysis, followed by the discrete phase model (DPM) for further computation and analysis. First, the rationality of the pure airflow field is verified, such as whether the velocity distribution adequately covers the workpiece surface; then, particles are introduced to analyze powder trajectories and deposition uniformity, thereby avoiding distortion in simulation results caused by airflow issues.

In single-phase flow analysis, since no particles are introduced, the focus is on studying gas pressure, velocity distribution, turbulence characteristics inside the nozzle or at the outlet, and the mechanical effects of the gas on the nozzle structure. Based on ANSYS FLUENT, the inlet velocity is set at 10 m/s. Fig 7. Displays the velocity and pressure contour plots of the simulated single-phase flow under identical conditions.

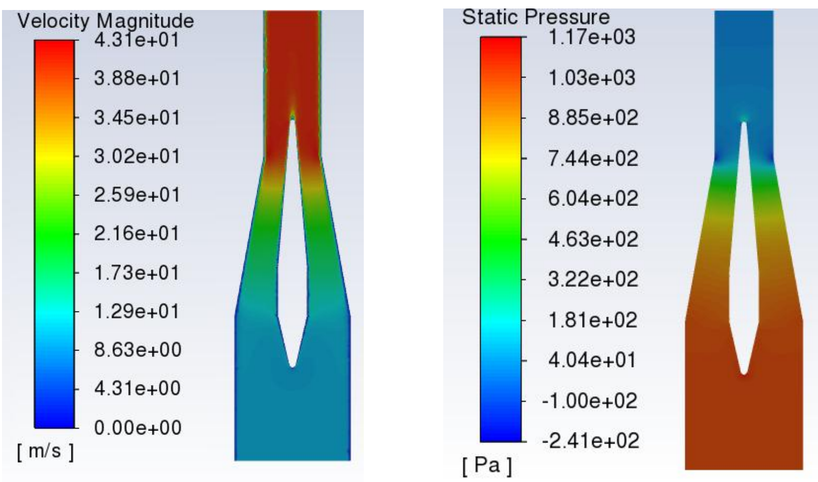

(a) Velocity Contour (b) Pressure Contour

Fig 7. Velocity and Pressure Contours of Single-Phase Flow.

By comparing airflow distribution diagrams in Fig 4, and 7. It is evident that the internal airflow of the optimized device is more uniform. In terms of airflow velocity, the improved electrostatic device exhibits faster airflow near the internal core than in other areas; this accelerated flow better facilitates powder movement and reduces accumulation in this region. Meanwhile, the air pressure in the unopened regions inside the nozzle remains consistent with the pre-optimized design, and this stable pressure environment reduces the likelihood of powder retention. In addition, the optimized airflow is not only more uniformly distributed but also flows more smoothly than before, indicating that the improved design ensures more rational and effective airflow.

The numerical simulation of single-phase flow primarily conducts a systematic study on the influence of spray gun structural parameters on the characteristics of gas-phase flow, while the discrete phase model focuses on exploring the interaction mechanisms between flow field characteristics and particle motion behavior under multiphase coupling conditions. When constructing the computational model based on the ANSYS FLUENT module, the discrete phase simulation inherits the geometric configuration and basic mesh system used in the single-phase flow study. Comparative analysis shows that applying local mesh refinement strategies in critical regions for particle transport, such as the spray gun outlet, can effectively enhance computational accuracy. The inlet velocity is also set at 10 m/s. Fig 8. Shows the velocity and pressure contour plots for the single-phase flow simulation.

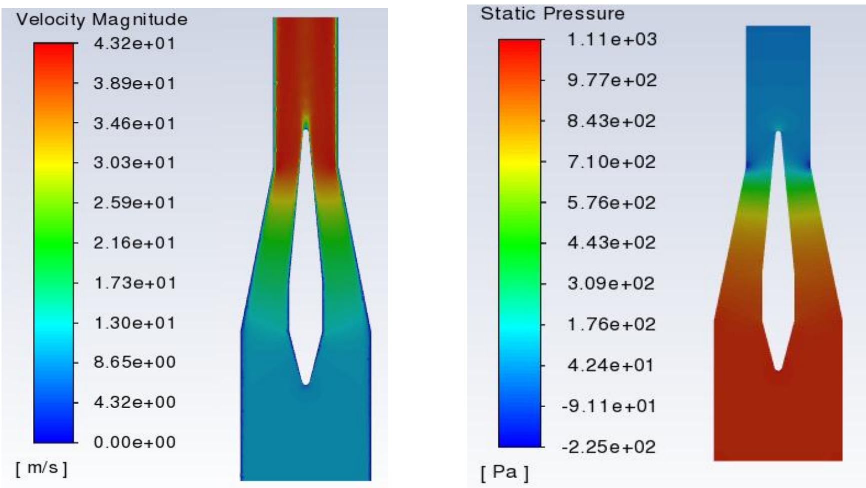

(a) Velocity Contour (b) Pressure Contour

Fig 8. Velocity and Pressure Contours of Discrete Phase Flow.

Building upon the preceding single-phase flow analysis, a comparative analysis of Fig 8. With the contour plots in Fig 3. Reveals substantial agreement between the single-phase flow results and the discrete phase model (DPM), while the contour plots in Fig 8. Demonstrate superior uniformity in their spatial distribution. From the velocity contour plots, the fluid velocity around the optimized electrostatic device's internal core is higher than that in other regions. As the powder travels with the airflow through this region at higher speed, it is less likely to accumulate in this area. From the pressure contour plots, the fluid pressure in the unopened areas inside the nozzle remains unchanged (pressure remains stable), which also reduces the likelihood of powder accumulation in these regions. In addition, compared to the pre-optimized design, the airflow is more stable and uniform, indicating a more rational airflow field after optimization. Theoretically, this demonstrates that the structural optimization has been successfully achieved.

3. Results and Analysis

3.1. Coating uniformity optimization

Through the structural optimization of the electrostatic device, numerical simulation results show that the new equilateral triangular topological configuration significantly improves the axial symmetry of the airflow field. Combined with the streamlined characteristics of the conical guide structure, it effectively enhances the concentration effect of powder particles in the central region. Compared with the original model, the optimized design exhibits smoother color transitions in the velocity cloud map and more uniform pressure distribution, indicating a significant improvement in spraying uniformity.

3.2. Durability and energy efficiency assessment

The design of three narrow crossbeams effectively disperses the stress distribution within the nozzle structure, reducing local stress concentration and thereby enhancing overall structural stability and durability. Meanwhile, the introduction of the conical structure allows for smoother flow channel transitions, reducing abrupt changes and turbulence within the channel, thereby lowering energy consumption and improving spraying efficiency. In addition, this optimized design not only improves nozzle performance but also significantly reduces maintenance costs. Reduced stress concentration and fewer abrupt changes in the flow channel result in less wear and fewer failures, thereby extending nozzle service life and reducing maintenance and replacement frequency.

4. Conclusions

This study provides a theoretical basis for the design of spray heads in spraying robots and offers an approach for nozzle optimization by thoroughly analyzing the interaction mechanisms between various physical fields. The principal conclusions drawn from this study are summarized as follows:

(1) The equilateral triangular distribution of the electrostatic device crossbeams combined with the conical inner cylinder design significantly improves the flow field characteristics and optimizes the powder accumulation issue.

(2) The optimized structure exhibits a rational stress distribution, a 59.8% reduction in deformation, and a maximum deformation below the safety threshold, significantly enhancing the durability and energy efficiency of the equipment.

(3) Fluid dynamics simulations validate the airflow stability of the optimized structure. Both single-phase flow and discrete phase models show a 31% improvement in the uniformity of velocity distribution at the nozzle outlet.

Future research should prioritize ambient-adaptive spraying strategy optimization through intelligent sensing systems. This involves developing a multi-physics coordination framework integrating real-time environmental monitoring modules with self-tuning control algorithms to dynamically synchronize electrostatic fields, airflow parameters, and thermo-hygrometric conditions. The system ensures coating uniformity while enhancing operational resilience under extreme conditions. Technical concurrency with advanced wear-resistant material development will deliver integrated solutions for nozzle durability and precision process control, ultimately enabling Industry 4.0-compliant coating systems

References

[1] Zhu D. Research and Application of Anti-Corrosion Treatment by Electrostatic Powder Spraying [J]. Chemical Engineering Design Communications, 2022, 48(06): 130-132.

[2] Wang Y. Research on high-voltage electrostatic powder coating technology [J]. Modern Industrial Economy and Informatization, 2022, 12(1): 144-146.

[3] Wang C., Liu Y., Zhang J. et al. Impact of VOC governance on the development of coating processes and equipment for construction machinery [J]. China Equipment Engineering, 2020, (S2): 234-236.

[4] Wang C., Han Y., Liu W. et al. Polyvinyl chloride/epoxy double layer powder coating enhances coating adhesion and anticorrosion protection of substrate [J]. Progress in Organic Coatings, 2021,158.

[5] Jiang R., Bi H., Zheng R. Analysis of Preparation Conditions of Low-Temperature Curing Powder Coatings Based on Local Clustering Algorithm[J]. Mathematical Problems in Engineering, 2022, 2022.

[6] Yang Q., Yuan F., Ma Y. et al. Electrostatic powder coated osmotic pump tablets: Influence factors of coating powder adhesion and film formation [J]. Powder Technology, 2020, 360444-451.

[7] Karaoglan AD., Ozden E. Electrostatic powder coating process optimisation by implementing design of experiments [J]. Transactions of the IMF, 2021, 99(1):46-52.

[8] Dominika JC., Kevin B., Barbara PP. et al Recent development advances in bio-based powder coatings: a review [J]. Journal of Coatings Technology and Research, 2023, 21(2):435-444.

[9] Zhang H., Guan T., Liu H. Structural Optimization of Spray Heads for Spraying Robots [J]. Light Industry Machinery, 2020, 38(05): 99-102.

[10] Chen W., Liu H., Hu Y., Liu C. et al. Research on the Powder Deposition Rate in Electrostatic Powder Spraying Based on Particle Size Distribution[J]. Coating Industry, 2021, 51(03): 71-75.

[11] Liu R., Zhou W., Ling W. et al. Performance optimization of ultra-low platinum loading membrane electrode assembly prepared by electrostatic spraying [J]. International Journal of Hydrogen Energy, 2021, 46(17):10457-10467.

[12] Boer J., Petruta B. Innovative Method to Reduce Process Costs in the Field of Electrostatic Powder Painting [J]. 2020, 46: 44-48.

[13] Wu D., Feng X., Chen Y. et al. Research on the Evaluation Method of Laboratory Capability for Testing the Tensile Yield Strength of Plastics [J]. New Building Materials, 2019, 46(4): 128-131.

[14] Huang W., Xiao T. Design of Ring Stiffness for Buried Plastic Drainage Pipes [J]. Municipal Technology, 2019, 37(02): 178-179.